Cerebral Cortex Advance Access published September 9, 2014

Cerebral Cortex
doi:10.1093/cercor/bhu200

Dendritic Excitability and Gain Control in Recurrent Cortical Microcircuits

Etay Hay[1] and Idan Segev[1,2]

[1]Edmond and Lily Safra Center for Brain Sciences and [2]Department of Neurobiology, The Hebrew University of Jerusalem, Jerusalem 91904, Israel

Address correspondence to Etay Hay. Email: etay.hay@mail.huji.ac.il

Layer 5 thick tufted pyramidal cells (TTCs) in the neocortex are particularly electrically complex, owing to their highly excitable dendrites. The interplay between dendritic nonlinearities and recurrent cortical microcircuit activity in shaping network response is largely unknown. We simulated detailed conductance-based models of TTCs forming recurrent microcircuits that were interconnected as found experimentally; the network was embedded in a realistic background synaptic activity. TTCs microcircuits significantly amplified brief thalamocortical inputs; this cortical gain was mediated by back-propagation activated *N*-methyl-D-aspartate depolarizations and dendritic back-propagation-activated Ca^{2+} spike firing, ignited by the coincidence of thalamic-activated somatic spike and local dendritic synaptic inputs, originating from the cortical microcircuit. Surprisingly, dendritic nonlinearities in TTCs microcircuits linearly multiplied thalamic inputs—amplifying them while maintaining input selectivity. Our findings indicate that dendritic nonlinearities are pivotal in controlling the gain and the computational functions of TTCs microcircuits, which serve as a dominant output source for the neocortex.

Keywords: active dendrites, cortical microcircuit, multiscale modeling, network simulation

Introduction

The response of neurons in the intact brain is dynamically influenced both by the local recurrent circuit activity and by nonlinear dendritic properties (Ben-Yishai et al. 1995; Liu et al. 2007; Takahashi and Magee 2009; Buesing et al. 2011; Larkum 2012; Xu et al. 2012; Li, Li et al. 2013; Li, Ibrahim et al. 2013; Reimann et al. 2013; Vaidya and Johnston 2013). This is particularly true for an important class of cortical neurons, the layer 5 (L5) thick tufted pyramidal cells (TTCs), as their dendritic tree is highly excitable (see below). Yet, the interplay between network activity due to recurrent connections and dendritic nonlinearity, and their combined effect on networks dynamics, is not well understood.

Previous studies of the modulation of response to sensory stimulus due to recurrent network activity considered network of L4 cells, which were thought to be the primary targets of thalamocortical axons (Gilbert and Wiesel 1979; Douglas and Martin 2004). In recent years, however, in vivo experiments have demonstrated a substantial direct thalamic input onto the perisomatic region of TTCs, resulting in postsynaptic potentials (PSPs) and spike latencies that were as early as those recorded in cells from L4 (Heimel et al. 2005; de Kock et al. 2007; Meyer et al. 2010; Constantinople and Bruno 2013). Therefore, investigation of the response of TTC network to direct thalamic input is highly relevant and presently lacking. Several recent experimental studies of excitatory cells in L4 in vivo indicate that, during auditory or visual sensation, the recurrent cortical network amplifies the response of these cells to thalamic input without changing their stimulus selectivity (Liu et al. 2007; Li, Li et al. 2013; Li, Ibrahim et al. 2013; Lien and Scanziani 2013). Previous theoretical studies showed that recurrent activity among cells that are similarly tuned to a stimulus property, such as visual orientation, could increase the response gain of the cells, thereby amplifying the response to thalamic input as well as sharpening the response selectivity or increasing signal-to-noise ratio (Ben-Yishai et al. 1995; Douglas et al. 1995; Suarez et al. 1995; Chance et al. 1999). In both the experimental and theoretical studies mentioned above, the contribution of dendritic excitability to the response modulation was not considered.

The major dendritic nonlinearities in TTCs involve Ca^{2+} spikes at the main bifurcation of the apical dendrites (Helmchen et al. 1999; Larkum and Zhu 2002; Xu et al. 2012) and *N*-methyl-D-aspartate (NMDA) spikes in thin branches of the apical and basal dendritic trees (Schiller et al. 2000; Rhodes 2006; Larkum et al. 2009; Polsky et al. 2009). Previous studies showed that NMDA spikes could amplify the cell's response as well as sharpen its selectivity (Lavzin et al. 2012; Smith et al. 2013; Palmer et al. 2014). NMDA conductance, in general, can act more locally to lower the threshold for Ca^{2+} spike generation (Schiller and Schiller 2001; Polsky et al. 2004; Larkum et al. 2009). Ca^{2+} spikes are longer and of higher amplitude than NMDA spikes. Recent in vivo experimental studies showed that disinhibiting the apical dendrites in TTCs drastically increases their response gain to somatosensory stimulation, in correlation with the dendritic Ca^{2+} signal (Murayama et al. 2009; Palmer et al. 2012). These findings complement earlier in vitro evidence for the influence of dendritic Ca^{2+} spikes on the frequency–current gain (Larkum et al. 2004). The effect of dendritic Ca^{2+} spikes on the cell's output (axonal) firing is particularly evident under coincident inputs to the soma and the distal apical dendrite, which correspond, respectively, to the thalamic (bottom-up) input and cortical (top-down or local) input that these cells receive in the intact brain (Felleman and Van Essen 1991; Constantinople and Bruno 2013). The coincidence of these 2 input sources triggers back-propagation-activated Ca^{2+} spike (BAC) firing in vitro (Larkum et al. 1999), which has been suggested to serve for neural computations such as cortical associations (Larkum 2012).

The involvement of dendritic Ca^{2+} spikes during coincidence of different streams of inputs was demonstrated experimentally in other brain regions as well. In the hippocampus, in vitro studies showed that coincident stimuli arriving at different regions of the dendrites triggered a Ca^{2+} plateau potential whose duration was correlated with synaptic potentiation (Ta-

kahashi and Magee 2009). During active whisking, the coincidence of motor and sensory input streams in L5 pyramidal cells triggers dendritic Ca^{2+} signals that are correlated with dendritic plateau potentials (Xu et al. 2012).

Several recent studies suggested that cortical networks may be regarded as composed of relatively small functional microcircuits, of tens to hundreds of cells (Perin et al. 2011). Connectivity in the cortex is not random, but rather involves a higher occurrence of interconnected microcircuits (or motifs) than expected by chance (Song et al. 2005; Perin et al. 2011), as well as a higher probability of connectivity between cells that share common inputs (Yoshimura et al. 2005; Kampa et al. 2006) or have a similar stimulus preference (Ko et al. 2011). Moreover, studies showed that cortical connectivity depends also on cell type (Yoshimura and Callaway 2005; Anderson et al. 2010). These studies indicated the existence of distinct microcircuits, which may act as functional modules. Understanding how such local cortical modules operate contributes to the understanding of the computational capabilities and function of larger networks composed of such modules (Traub et al. 2005; Douglas and Martin 2007; Heinzle et al. 2007, 2010; Buonomano and Maass 2009; Litvak and Ullman 2009; Papoutsi et al. 2013).

In order to explore the combined contribution of both the recurrent cortical network activity and of dendritic excitability to the modulation of thalamocortical inputs, we simulated cortical microcircuits composed of detailed TTCs, using the novel detailed model for TTCs that we had recently developed (Hay et al. 2011). These local cortical networks were immersed in the context of in vivo-like background activity. We show that the modulation of response in TTC microcircuits by recurrent activity following somatic ("bottom up") input relies heavily on back-propagating action potential (BAP) boosting of dendritic excitatory postsynaptic potentials (EPSPs), triggering NMDA currents, and BAC firing. Namely, the dendritic properties of TTCs had a significant role in shaping the dynamical response of the local excitatory network. Using orientation tuning as an example, we illustrated the possible functional meaning of these 2 mechanisms for modulating the response of excitatory cortical networks.

Materials and Methods

Single-Cell Model

Each TTC in the microcircuit was represented using the detailed conductance-based model that we have recently developed (Hay et al. 2011). This model exhibited somatic Na^+ spike firing, dendritic Ca^{2+} spike, BAP due to dendritic Na^+ channels and a burst of somatic Na^+ spikes in response to the coincidence depolarization to the soma and the apical tuft (the BAC firing, see Larkum et al. 1999). The modeled microcircuit in the present study was composed of $N = 1$–150 of these modeled cells, all identical in their morphology and biophysical properties.

Background Synaptic Input

In order to simulate the circuit in the context of in vivo activity, we randomly distributed 10 000 excitatory synapses and 2500 inhibitory synapses on each TTC model as suggested by previous careful estimates in cat neurons (Binzegger et al. 2004). We note that possible difference in estimates for rat neurons due to a difference in cell size were not crucial for our investigation, as it could be compensated for by changing the ratio of the inhibitory and excitatory conductances. Every excitatory synapse included a combination of NMDA- and AMPA-dependent conductances as well as unified short-term plasticity dynamics (Ramaswamy et al. 2012), with equal maximal conductance (Sarid et al. 2007). The rise time constant of NMDA conductance was 2 ms and its decay time constant was 65 ms (Rhodes 2006). The rise time constant of AMPA conductance was 0.3 ms and its decay time constant was 3 ms (Hestrin 1992). The inhibitory synapses were of the $GABA_A$ type. The rise time constant of $GABA_A$ conductance was 1 ms and its decay time constant was 20 ms (Salin and Prince 1996; Gidon and Segev 2012). The reversal potentials of the excitatory and inhibitory synapses were 0 and −80 mV, respectively (Destexhe et al. 1994), and the resting potential of the modeled cells was −80 mV. Both inhibitory and excitatory synapses had probabilistic release with short-term plasticity (Ramaswamy et al. 2012). The mechanism accounting for the combined AMPA and NMDA currents had a short-term depression, with a release probability (U) of 0.6, time constant of recovery from depression (D) of 800 ms and time constant of recovery from facilitation (F) of 0 ms (Tsodyks and Markram 1997; Fuhrmann et al. 2002). The inhibitory synapses were depressing as well, with $U = 0.25$, $D = 800$ ms, and $F = 0$ ms (Gupta et al. 2000).

We set the maximal inhibitory synapse conductance to 1 nS, yielding an average somatic inhibitory postsynaptic potential (IPSP) amplitude of −0.6 mV at holding membrane potential of −70 mV for an inhibitory connection consisting of 12 synaptic contacts (Silberberg and Markram 2007). The maximal conductance for NMDA- and AMPA-receptors was 0.4 nS, yielding an average EPSP amplitude of 0.6 mV at the resting potential (Song et al. 2005; Thomson and Lamy 2007; Perin et al. 2011) for an excitatory connection (single TTC axon) making 5 synaptic contacts on a single target TTC dendrite (Markram et al. 1997). Background presynaptic trains of action potentials (APs) followed a Poisson distribution, with average firing rate of 0.72 Hz for the excitatory synapses (Heimel et al. 2005) and 7 Hz for the inhibitory synapses (Gentet et al. 2010). These settings yielded a spontaneous firing rate of 3.1 ± 0.5 Hz in unconnected TTCs (microcircuit size $N = 1$), and 4.3 ± 1.5 Hz in the TTCs composing microcircuits of size $N = 150$, both on the order of magnitude found in vivo (Heimel et al. 2005; Olsen et al. 2012). In addition, this setting yielded a normal distribution of the subthreshold membrane potential, with mean of −63 mV and standard deviation of 3 mV, in agreement with experimental measurements in awake animals (Constantinople and Bruno 2011).

Microcircuit Connectivity

TTCs were connected to each other with a probability $P = 0.13$ for unidirectional connections and a probability of $P_{rcp} = 0.06$ for reciprocal connections (Song et al. 2005). Reciprocal connections were 1.5 times stronger (larger synaptic conductance) than unidirectional connections (Song et al. 2005). The delay between presynaptic AP onset at soma and beginning of postsynaptic EPSP was 1 ms (Markram et al. 1997). Each connection consisted of 5 synaptic contacts of the NMDA/AMPA type (modeled as for the excitatory background connections described above), except that these synapses were facilitating, with $U = 0.25$, $D = 0$ ms, $F = 0$ ms (Reyes and Sakmann 1999; Frick et al. 2007; Williams and Atkinson 2007). Although studies showed that synaptic locations between TTCs tend to contact the basal and oblique dendrites, they can occur all along the dendritic tree of the postsynaptic cell (Markram et al. 1997). We thus distributed the different synaptic contacts from the presynaptic microcircuit cells randomly on each postsynaptic cell. In gathering firing statistics for microcircuits of size N, we simulated 4 different random microcircuits for each case. The microcircuits differed in the connectivity between TTCs, in the synaptic locations of connections between TTCs and in the presynaptic trains of the background input impinging on each TTC. We did not analyze microcircuits of size larger than $N = 150$ cells, since under the conditions of the present study the spontaneous rate in such microcircuits diverged significantly from the experimentally measured spontaneous rate.

Post-Stimulus Time Histogram

In producing post-stimulus time histogram (PSTH), we binned the simulated voltage traces of all cells within the network to bins of 5 ms. Each bin received a value of 1 if it contained a spike onset or a value of 0 otherwise.

Visual Orientation Selectivity

We emulated stimuli of different visual orientations by using different amplitudes of the brief (5 ms) depolarizing pulse injected to the soma of all modeled cells, between 0 nA (corresponding to no bottom-up thalamic input, or the "null orientation") to 1.4 nA (our default amplitude in this study, which induced exactly 1 extra spike in all microcircuit cells, and corresponded to "preferred orientation"). The spike response rates in the null and preferred orientations were on the order of magnitude seen experimentally (Van Hooser 2007). The intermediate pulse amplitudes were 0.2, 0.4, and 0.6 nA, yielding response rates within the circuit that spanned the range between the responses to the null and the preferred orientations. We then derived the corresponding stimulus orientation angles, using a Gaussian response curve that had half-width at half-height of 29°, in agreement with experimental statistics (Van Hooser 2007). The center of the response curve corresponded to the preferred orientation, which was arbitrarily assigned to be 90°. To quantify the orientation selectivity we used 2 measures, the half-width at half-height and the selectivity index, which is the ratio between the second and first Fourier components of the orientation curve (Ringach et al. 2002). We note that the choice of emulating stimuli with brief currents rather than detailed synaptic input served to (i) trigger a somatic spike robustly and (ii) keep the analysis at the fundamental level of response-current (*f–I*), thereby allowing our findings to benefit from being general and not tied to specific assumptions regarding the synaptic input.

All simulations were conducted using NEURON (Carnevale and Hines 2006), running on a grid of 60 Sun X4100 AMD 64 bit Opteron dual core (240 cores in total), running Linux 2.6. Average runtime of each microcircuit simulation (of N neurons using N cores) was 30 min. The simulation code is available at ModelDB (Hines et al. 2004).

Results

In order to study network dynamics within a realistic recurrent network of TTCs, we connected microcircuits composed of 1–150 detailed TTCs models (see Materials and Methods). Figure 1*A* illustrates an example microcircuit of 50 cells, with unidirectional (black lines) and reciprocal (red lines) connection probabilities as found experimentally (see Materials and Methods). In addition to connections from the microcircuit, each cell received random Poisson background inhibitory and excitatory synaptic inputs that caused it to fire spontaneously at an acceptable range of rates in all of the microcircuit sizes we examined (Fig. 1*B*). Unconnected cells (microcircuit size $N = 1$) fired spontaneously at 3.1 ± 0.5 Hz, and cells in microcircuits of size $N = 150$ fired spontaneously at 4.3 ± 1.5 Hz, both within the experimental range as found in the neocortex (see

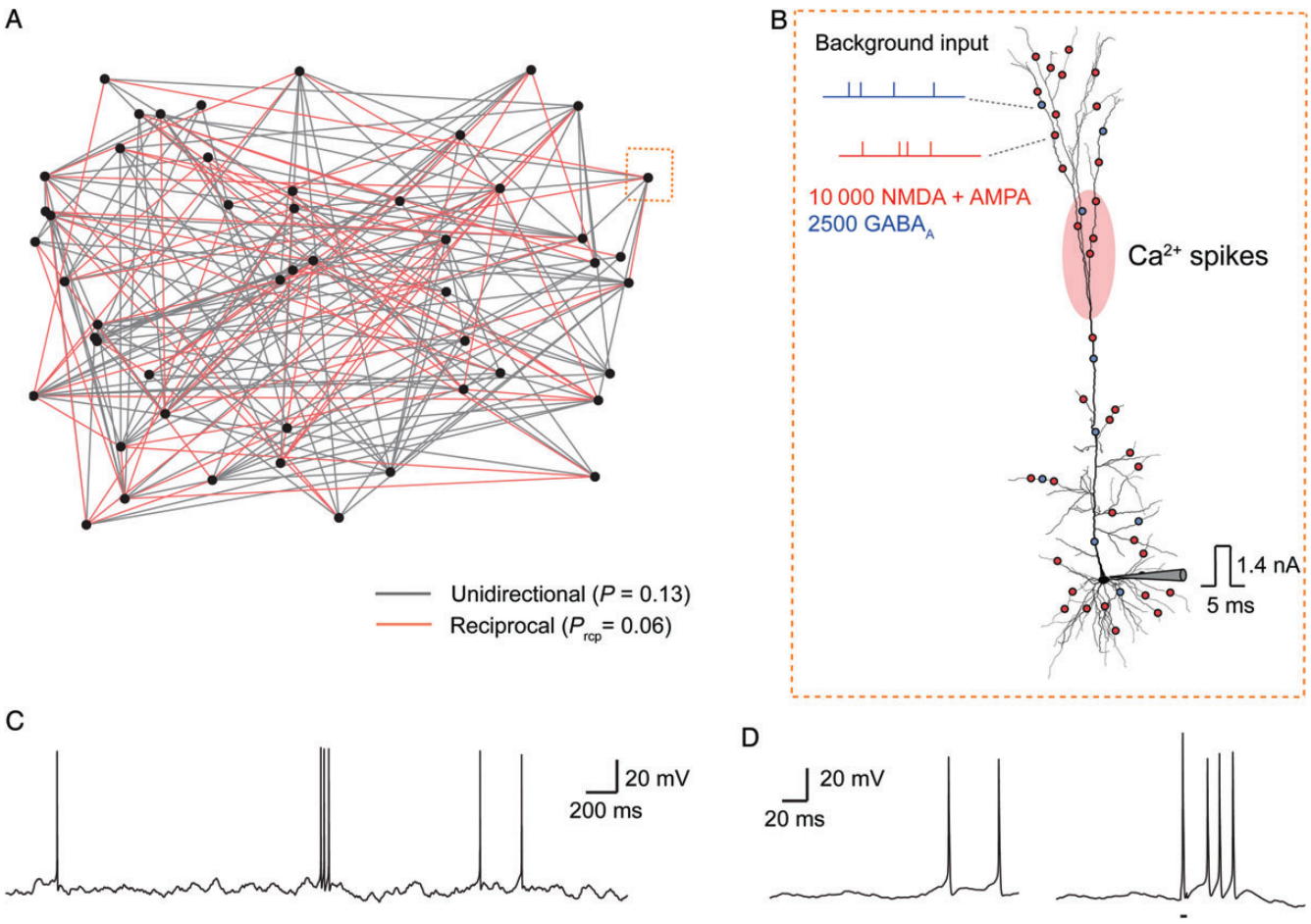

Figure 1. Simulated TTCs microcircuits. (*A*) An exemplar microcircuit of 50 cells. Connection probabilities between cells were 0.13 for unidirectional connections (black edges), and 0.06 for reciprocal connections (red edges). Reciprocal excitatory synaptic connections were 1.5 times stronger than unidirectional connections. (*B*) An example of a modeled TTC, with its detailed morphology, receiving a background Poisson input from 10 000 excitatory synapses (red) and 2500 inhibitory (blue) synapses (see Materials and Methods). On top of this background input, all cells in the microcircuit were simultaneously stimulated by a brief somatic current input of 1.4 nA and 5 ms duration (black electrode), mimicking a brief perisomatic thalamic input. In addition to firing somatic Na^+ APs, the TTC model was capable of generating dendritic Ca^{2+} spikes at the apical "hot zone" (shaded red ellipse). (*C*) Spontaneous firing of an exemplar single (isolated) TTC in response to the background synaptic input. (*D*) Voltage traces of another example cell, from a microcircuit of 150 cells, firing spontaneously (2 spikes, left) and in response to simultaneous somatic input to all network cells (4 spikes, right). Stimulus is indicated by black bar below the voltage trace.

Materials and Methods). An example of the spontaneous firing is shown in Figure 1*C*.

We were first interested in the activity in cells following a single somatic spike induced synchronously in all cells. We therefore applied a brief (5 ms) suprathreshold somatic input of 1.4 nA to all cells in the circuit (example trace is depicted in Fig. 1*D*). Single (unconnected) cells responded to this somatic input with a single spike locked to the stimulus time, $t = 0$, with no subsequent increase in firing rate above the base rate (Fig. 2*A*). In contrast, in microcircuits of 150 cells, the somatic stimuli triggered increased activity in the circuit for duration of ~70 ms, after which the activity returned to baseline rate (Fig. 2*B*). We focused the analysis on a time window of 50 ms following stimulus onset ($t = 0$–50 ms), and calculated the average firing rate in microcircuits of $N = 150$ cells to be 47.1 ± 3.9 Hz for this time window. The average response firing rate in single unconnected cells during the 50 ms window was 22.1 ± 0.7 Hz.

In order to determine the extent by which dendritic excitability contributed to the microcircuit activity, we examined similar microcircuits in which particular dendritic channels or NMDA receptors were removed. We note that removing NMDA receptors was done by setting the rise and decay time constants of the NMDA component in the excitatory synapse mechanism to be infinitesimally small. In addition, when we removed NMDA receptors we increased the maximal excitatory conductance to keep the spontaneous rates unchanged. Removing dendritic Na^+ channels essentially abolished the prolonged increase in network activity after the first induced spike, so that the average response in microcircuits of $N = 150$ cells was 24.7 ± 1 Hz (Fig. 2*C*), only slightly higher than the response of unconnected cells (22.1 ± 0.7 Hz). Removing dendritic Ca^{2+} channels reduced the microcircuit response to 41.1 ± 2.8 Hz (Fig. 2*D*, red curve), a 13% decrease of the rate compared with control conditions (see above). Removing only high-voltage-activated dendritic Ca^{2+} channels resulted in a similar effect (Fig. 2*D*, green curve), whereas removing low-voltage-activated dendritic Ca^{2+} channels had no significant effect (not shown). Blocking Na^+ channels or NMDA receptors had a similar effect, abolishing the prolonged increase in network activity after the second spike (Fig. 2*D*, purple and blue, respectively). This limited recurrent activity in the microcircuits with nonexcitable dendrites is expected due to their small size and the low connection probability between cells, and since all TTCs in the connected network receive simultaneous somatic input (as single additional spike), which could not propagate effectively through the network due to the refractoriness in all cells

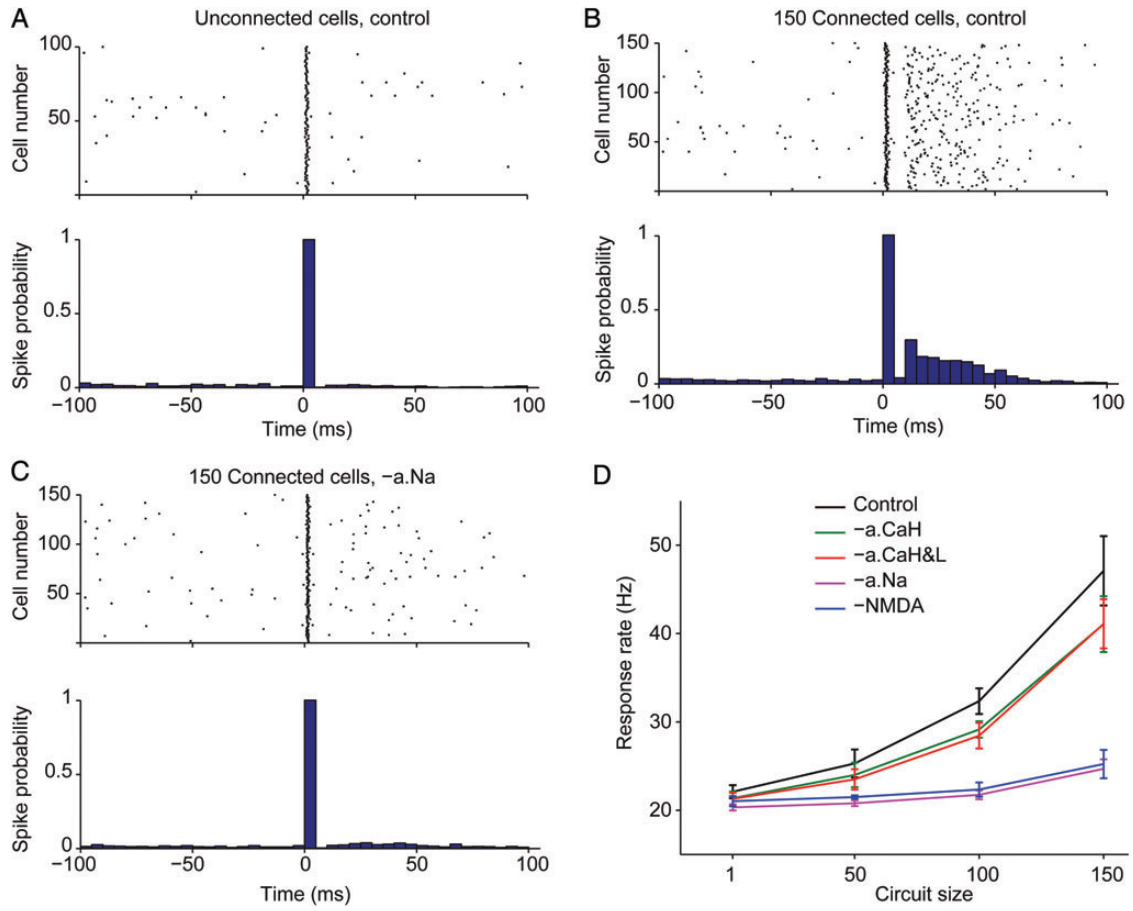

Figure 2. Modulation of response rate by recurrent activity and dendritic excitability. (*A*) An example raster plot (top) and PSTH (bottom) of the firing of single (unconnected) cells in response to brief suprathreshold somatic/thalamic input at $t = 0$ (stimulus as in Fig. 1*B*). (*B*) Example raster plot (top) and PSTH (bottom) for the response to somatic input in microcircuits of $N = 150$ cells, all receiving brief suprathreshold somatic input at $t = 0$. (*C*) Same as in (*B*), except that apical dendritic Na^+ channels in modeled cells were removed (denoted: −a.Na). (*D*) Response rate of cells in microcircuits of size $N = 1$–150 cells, in control condition as in (*B*) (black curve) and when removing particular apical dendritic channels (high-voltage-gated Ca^{2+} channels, green curve; both high- and low-voltage-gated Ca^{2+} channels, red curve; Na^+ channels, purple curve) or NMDA receptors on both basal and apical dendrites (blue curve). The instantaneous rate was measured in a time window of 50 ms following stimulus onset.

following this spike. We note that removal of dendritic Ca^{2+} and Na^+ channels reduced spontaneous firing (2.6 ± 0.5 Hz compared with 4.3 ± 1.5 Hz in control conditions in microcircuits of 150 cells). However, both of these rates were within the physiological range (see Materials and Methods). We also note that the variability in response or spontaneous firing rate is as observed in vivo (Heimel et al. 2005).

The recurrent activity and dendritic excitability in microcircuits of $N = 150$ cells with fully excitable dendrites resulted in a response rate that was 2.3 times larger than the response rate of single (unconnected) cells with no dendritic Na^+ channels (47.1 ± 3.9 Hz vs. 20.3 ± 0.4 Hz, Fig. 2*D*). The response rate increased supralinearly as a function of the number of cells in the microcircuit (Fig. 2*D*, black curve), but increased only little with the number of cells in microcircuits with nonexcitable dendrites (Fig. 2*D*, purple or blue curves). Taken together, these results demonstrate that both dendritic excitability and microcircuit recurrent activity contributed to the observed modulation of response rate. From Figure 2*D* it is apparent that the dendritic nonlinearity has a major role in enhancing network activity following simultaneous suprathreshold somatic stimulation (mimicking a brief perisomatic thalamic input).

We investigated further the involvement of dendritic voltage-dependent ion channels and NMDA receptors in shaping the network firing response, by examining dendritic and somatic voltage traces in microcircuits of $N = 150$ cells. For an exemplar cell (Fig. 3*A*) in control conditions, following the brief somatic/thalamic input, there was a large depolarization at the main apical bifurcation, which lasted ~70 ms after the somatic stimulus has ended. This dendritic depolarization was typically accompanied by a burst of 2 additional spikes at the soma. The dendritic depolarization was in the order of magnitude and duration of Ca^{2+} spikes during BAC firing observed in vitro (Larkum et al. 1999, 2004; Hay et al. 2011). The addition of 2 somatic spikes with a short interspike interval (<30 ms) was typical to BAC firing as well. When dendritic Ca^{2+} channels were removed, the dendritic depolarization was reduced considerably and so was one of the additional somatic Na^+ spikes (Fig. 3*B*), thereby confirming that the dendritic depolarization and increase in somatic response were mediated partly by the voltage-gated dendritic Ca^{2+} channels. When NMDA receptors were also removed, the dendritic depolarization was abolished and with it the additional somatic Na^+ spike (Fig. 3*C*). The remaining dendritic depolarization was due to the EPSPs coming from the microcircuit. Removing only dendritic Na^+ channels was sufficient to abolish the dendritic depolarization and somatic spikes (Fig. 3*D*). Taken together, these results show that in control conditions the BAP (mediated by dendritic Na^+ channels) triggered NMDA depolarization and BAC firing, in agreement with recent studies (Larkum et al. 2009).

Characterizing the contribution and nonlinear nature of dendritic phenomena is harder under synaptic noise than it is in quiescent conditions. Nevertheless, a distribution of the dendritic voltage integral over $t = 0$–50 ms, in microcircuits of 150 cells receiving simultaneous somatic input, illustrates the dendritic events during network activity (Fig. 3*E*). In control conditions, there was a large dendritic depolarization whose magnitude in the different cells exhibited a bimodal distribution with one peak ~500 mV ms and another peak ~1300 mV ms, indicating a strong supralinear dendritic event in some of the cells (Fig. 3*E*, black curve). Particularly large integral values (>800 mV ms) occurred in 55% of the cells and reflected dendritic depolarization with duration and magnitude typical of Ca^{2+} spikes, such as seen in Figure 3*A*. Apparently, for these cells, the input conditions (both spatially and temporally) happened to be favorable for triggering of strong dendritic nonlinearities. When dendritic Ca^{2+} channels were removed, the distribution of dendritic voltage integral was unimodal and

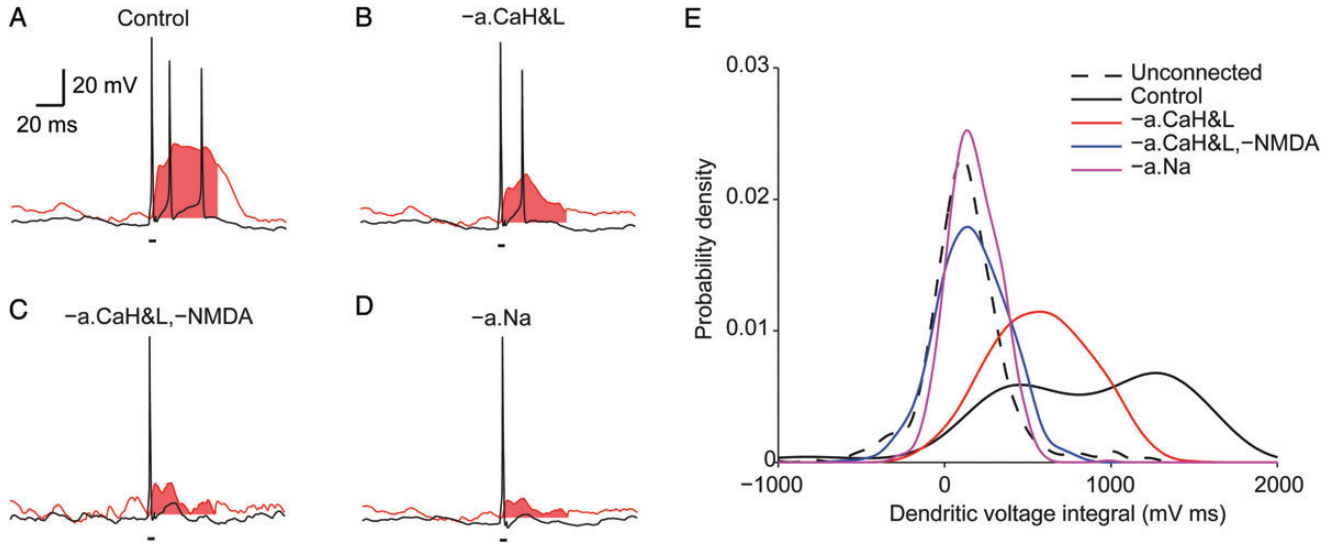

Figure 3. Microcircuit response involves strong dendritic nonlinearities. (*A*) Voltage traces at the soma (black) and at the apical main bifurcation (650 μm from the soma, red, see scheme in Fig. 1*B*) of an exemplar cell. The cell was part of a microcircuit of size $N = 150$ cells, receiving a brief suprathreshold somatic input to all circuit cells in control conditions. Somatic stimulus at $t = 0$ is indicated by black bar below the trace. The area under the dendritic voltage response, for $t = 0$–50 ms, is shaded in red. (*B–D*) Same as (*A*), but for the cases when the dendritic Ca^{2+} channels were removed (*B*), or also NMDA receptors were removed (*C*), or only dendritic Na^+ channels were removed (*D*). (*E*) Distribution of the integral of the membrane depolarization at the apical main bifurcation over the 50 ms time window in all cells from microcircuits of 150 cells from 4 different randomized simulations ($n = 600$ cells for each curve, see Materials and Methods), receiving simultaneous somatic input, under control conditions (solid black curve), when dendritic Ca^{2+} channels were removed (red curve), when also NMDA channels were removed (blue curve), or when only dendritic Na^+ channels were removed (purple curve). The distribution for unconnected cells under control conditions is shown by the dashed black curve ($n = 400$ cells). The bimodal distribution for the solid black curve indicates nonlinear dendritic events.

700 mV ms on average (Fig. 3*E*, red curve). When NMDA receptors were also removed, or when dendritic Na^+ ion channels alone were removed, the dendritic depolarization average was reduced to 100 mV ms and was never >700 mV ms, indicating a weak and essentially linear dendritic electrical behavior (Fig. 3*E*, blue and purple curves, respectively). For unconnected cells, where there was no significant activity beyond the induced somatic spike (Fig. 2*A*), most cells showed a unimodal distribution of dendritic voltage integral, centered ~100 mV ms as well. A large dendritic depolarization occurred only rarely in unconnected cells (in <3% of the cells), when the background input itself happened to be sufficient for triggering BAC firing (Fig. 3*E*, dashed black curve).

As not all cells in a cortical circuit are likely to receive the thalamic input at the exact same time, we examined the effect of temporal noise in the input on our results, by applying a random jitter of 10 ms to the somatic stimulus onset (i.e., the onset could be at any time point between $t = 0$ and $t = 10$ ms). Figure 4*A* shows a raster plot and PSTH in microcircuits of 150 cells under this noisy condition. A clear difference from the non-noisy condition (Fig. 2*B*) was the absence of uniform spiking across all cells at time $t = 0$ ms, since the somatic stimulus could occur anywhere between 0 and 10 ms. The response rate in microcircuits of 150 cells was 2.1 times larger than the response rate of isolated cells with no dendritic Na^+ channels (43.2 ± 2.8 Hz vs. 20.5 ± 0.4 Hz, Fig. 4*B*). Therefore, even under temporal noise in the thalamic input, the modulation of response rate due to dendritic nonlinearities and recurrent network activity remained robust and similar in magnitude to the amplification in control conditions (without jitter). As before, the contribution of both dendritic excitability and recurrent connectivity were necessary for the observed modulation, since the response was low in single cells or in microcircuits of cells with nonexcitable dendrites (compare Figs 2*D* and 4*B*). Dendritic nonlinearities and BAC firing occurred in the noisy input condition as well, as demonstrated by the bimodal distribution of dendritic depolarization integral (Fig. 4*C*, solid black curve). The portion of cells exhibiting large dendritic depolarizations (dendritic integral >800 mV ms) was slightly reduced, 44% compared with 55% in the nonjittering case (see above). As in the nonjittering case, removing dendritic Ca^{2+} channels abolished BAC firing in connected cells (Fig. 4*C*, red curve), and removing dendritic Na^+ channels abolished the dendritic depolarization (Fig. 4*C*, purple curve). Similarly, for jittery input, unconnected cells (microcircuit size $N = 1$) showed only a negligible modulation of response rate due to dendritic excitability (Fig. 4*B*) and did not commonly exhibit BAC firing or NMDA depolarizations (Fig. 4*C*, dashed black curve).

We have also examined the case where only part the microcircuits of 150 cells received the thalamic input (Fig. 5). In the fully excitable network, the response rate increased linearly with number of cells activated (Fig. 5*B*). Figure 5*B* also shows that dendritic nonlinearity kicks in even when a small percentage of the cells are activated via the thalamic input (compare black and color lines).

The computational consequence of the response modulation due dendritic excitability and recurrent activity depicted above could be utilized for amplifying and/or shaping the response selectivity of the cortical cells to the thalamic input (Douglas et al. 1995; Liu et al. 2007; Li, Li et al. 2013; Li, Ibrahim et al. 2013; Lien and Scanziani 2013). We examined these possibilities using our TTCs network by emulating a visual input of different orientations arriving from the thalamus. Different visual orientations were emulated by varying the amplitude of the brief (5 ms) pulse representing thalamic input (see Materials and Methods). In control conditions with excitable dendrites, the response in microcircuits of 150 cells was amplified by a factor of 2.3 compared with the response of single unconnected cells (Fig. 6*A*, solid vs. dashed black curves). However, there was no change in selectivity (in the shape of the tuning curve) of the cells (Fig. 6*B*, solid vs. dashed black curves). Namely, the network had a multiplicative effect which scaled the tuning curve similarly for all input angles.

We quantified the selectivity in each case using half-width at half-height, which characterizes the selectivity around the preferred orientation; and also used a selectivity index, which is a more global measure of selectivity (see Materials and Methods). In both cases, cells had an average tuning half-width at half-height of 29°, around a preferred angle (arbitrarily assigned to be 90°). The selectivity index was slightly smaller in unconnected cells compared with that in microcircuits of 150 cells (0.45 vs. 0.53, respectively), due to the reduction in the

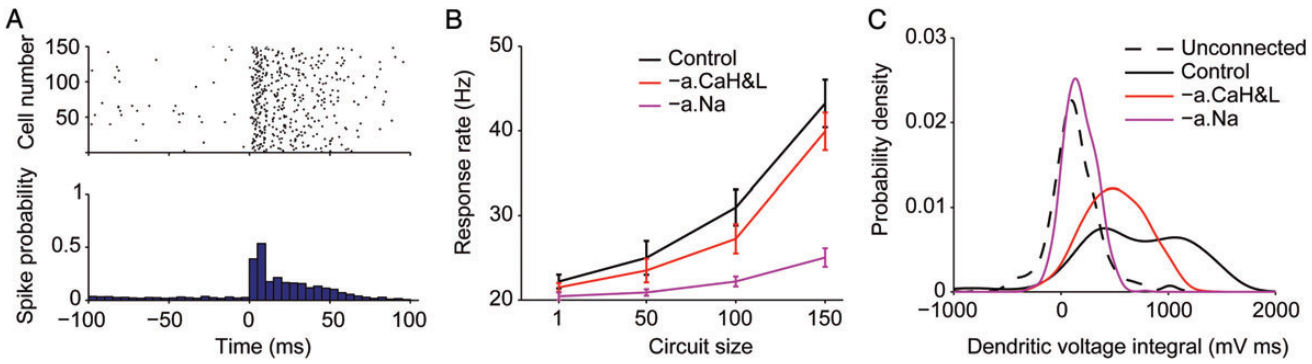

Figure 4. Modulation of network response by recurrent activity and dendritic excitability is robust to temporal noise in the thalamic input. (*A*) Raster plot (top) and PSTH (bottom) for microcircuits of 150 cells, receiving brief suprathreshold somatic input, with a random jitter of 0–10 ms in the onset of the somatic stimulus. (*B*) Response of cells in microcircuits of size $N = 1$–150 receiving somatic input with 0–10 ms jitter, in control conditions (black curve) and when dendritic Ca^{2+} or Na^+ channels were removed (red and purple curves). (*C*) Distribution of voltage integral at the main apical bifurcation in all cells from microcircuits of 150 cells ($n = 600$), receiving jittered somatic input, under control conditions (solid black curve) and when dendritic Ca^{2+} or Na^+ channels were removed (red and purple curves). The distribution of dendritic integral for unconnected cells is given by the dashed black curve ($n = 400$).

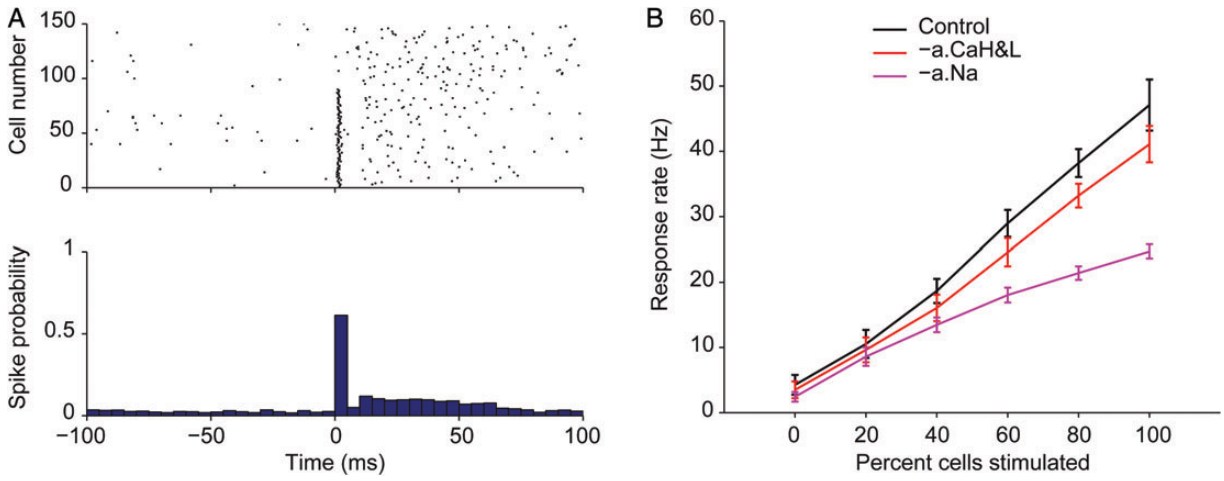

Figure 5. Microcircuit response to a partial thalamic input. (*A*) Example raster plot (top) and PSTH (bottom) for the response to somatic/thalamic input given to 60% of the cells in microcircuits consisting of 150 cells. (*B*) The response rate in microcircuits of 150 cells as a function of the percent of cells stimulated, in control conditions (black curve) and when dendritic Ca^{2+} or Na^{+} channels were removed (red and purple curves).

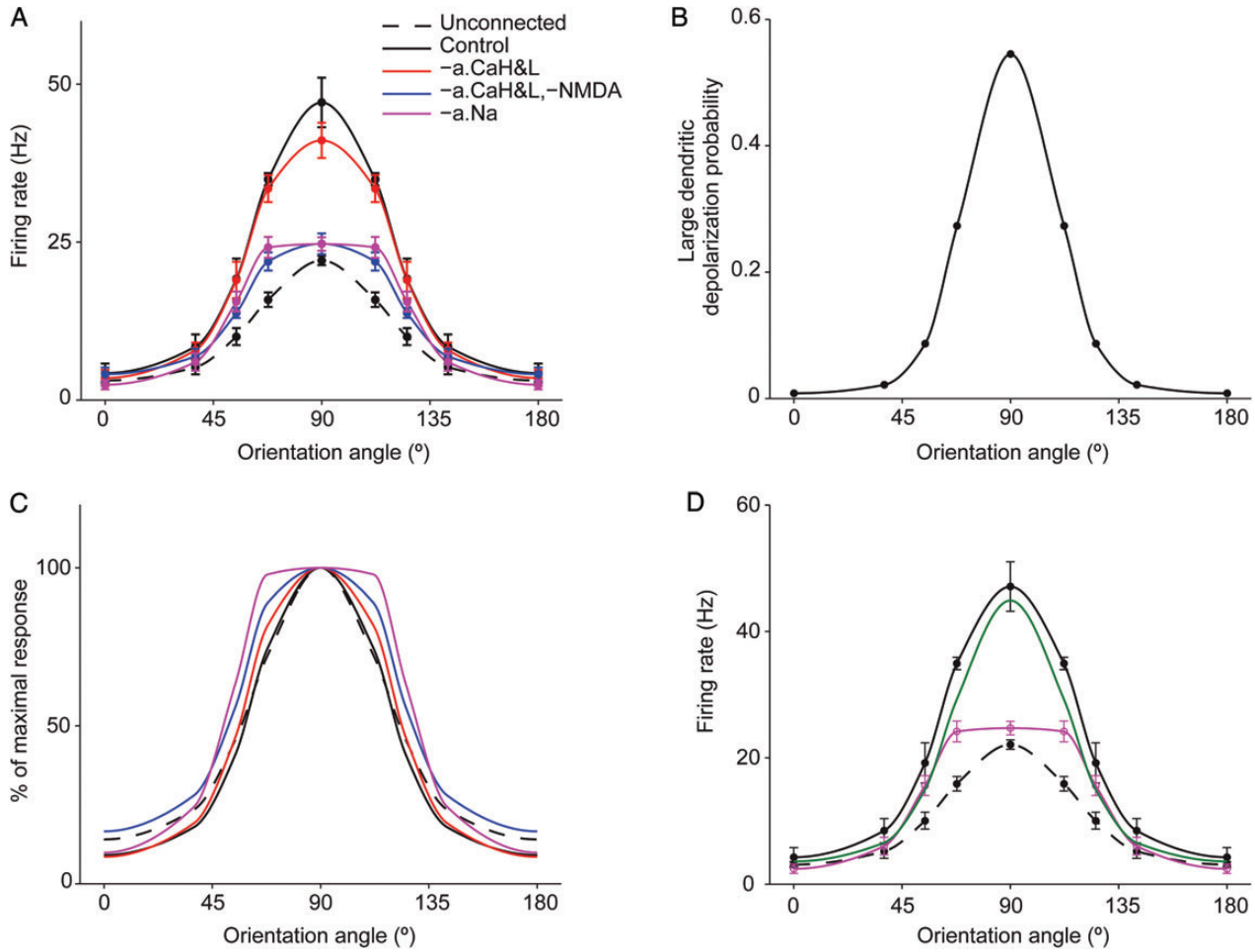

Figure 6. Dendritic excitability and recurrent activity amplify response to thalamic input while maintaining selectivity. (*A*) The average response in microcircuits of 150 cells (solid curves) or in unconnected cells (dashed black curve) to different somatic pulse amplitudes, reflecting different stimulus orientations (see Materials and Methods). Control conditions are depicted by the black curves whereas color curves are for the cases when dendritic Ca^{2+} or Na^{+} channels, or also NMDA receptors were removed. (*B*) Normalized response curves taken from (*A*). (*C*) The probability of large dendritic depolarizations in microcircuits of 150 cells increased with stimulus orientation towards the preferred orientation (90°). Large dendritic depolarization was defined to be the case when the dendritic voltage integral at the main apical bifurcation was >800 mV ms. (*D*) The predicted response rate in microcircuits of 150 cells based on the probability of obtaining large dendritic depolarization, as a function of orientation (given in *C*) is shown by the green line. Purple and black curves are as in (*A*).

difference between normalized responses to preferred and null orientations.

Interestingly, when dendritic Na^+ channels were removed, the amplification was abolished and the average tuning curve in microcircuits 150 cells was broadened in a nonuniform manner (Fig. 6*A*,*B*, purple curve). The central part of the curve (around the preferred orientation) flattened out, resulting in microcircuit that responded similarly to all angles between 70° and 110°. The tuning half-width at half-height increased from 29° to 39°. The global selectivity index was only slightly reduced in that case (0.48 compared with 0.53 in control), due to the sharpness of the curve. Therefore, removal of excitable channels from the dendrites in microcircuits of 150 cells resulted in a general decrease of 35% in selectivity as well as in a complete abolishment of selectivity for angles within 20° from the original preferred orientation. In contrast, removing dendritic channels in single unconnected cells did not change their selectivity (not shown). The small and broad amplification due to recurrent microcircuit activity in the case of removed dendritic Na^+ channels leveled off ~22 Hz (Fig. 6*A*, purple curve). Thus, the recurrent activity brought to threshold all the cells in which non-preferred angles (weaker thalamic stimuli) were insufficient to trigger firing, resulting in all microcircuit cells firing a single AP (equivalent to an average response rate of ~20 Hz in the 50 ms time window) for a broad range of angles around the preferred orientation. As noted above, recurrent activity alone (without dendritic excitability) was not effective for triggering more than a single spike per cell for reasons of spike refractoriness and low probability of connections between cells in the microcircuit. Therefore, in the amplification of response by cortical microcircuits, dendritic excitability was crucial for amplifying the response rate in a manner that maintained the stimulus selectivity induced in the single cells. Removing dendritic Ca^{2+} channels partly decreased the amplification and increased the tuning width (Fig. 6*A*,*B*, red curve), whereas removing also NMDA receptors further broadened the tuning width to a similar extent seen when removing dendritic Na^+ channels (Fig. 6*A*,*B*, blue curve). In this case, the top part of the curve was not flattened, indicating that dendritic Na^+ channels contributed directly to the boosting of somatic response near the preferred orientations.

The involvement of dendritic excitability in counteracting the broad amplification due to recurrent activity was also evident by the relation between probability of attaining large dendritic depolarization (dendritic voltage integral >800 mV ms, either via NMDA or BAC firing) and the stimulus orientation in microcircuits of 150 cells (Fig. 6*C*). At the preferred orientation (90°) the probability to attain large dendritic depolarization was 55%, and dropped almost linearly to a low probability of 1% at orientations further away than 45° from the preferred orientation. This indicated that dendritic excitability amplified the response to a larger extent as the stimulus orientation was closer to the preferred orientation. Indeed, assuming a burst of 3 APs during BAC firing, the predicted response rate due to this increase in the probability of large dendritic depolarization accounted well for the sharp selectivity compared with that in the nonexcitable dendrites case (Fig. 6*D*, green line vs. purple line).

Simulating the thalamic input using EPSP shaped somatic current (rather than a brief current pulse), with decay time constant of 5 ms (Constantinople and Bruno 2013), or replacing the somatic stimulus by a combination of somatic stimulus and dendritic stimulus at the main bifurcation did not significantly change the results (not shown). We note that since the amplification effect is roughly proportional to the change in the gain between maximal and minimal response, the magnitude of amplification should vary with microcircuit size as the response rates shown in Figure 2*D*.

Discussion

By analyzing recurrent microcircuits of detailed interconnected L5 thick tufted cells receiving thalamic input, we provided the first indication that dendritic excitability contributes significantly to the network modulation of the response to bottom-up (thalamic) input. We showed that a significant part of this modulation was mediated by BAP triggering NMDA nonlinearities as well as BAC firing (Larkum et al. 1999; Stuart and Hausser 2001) due to coincidence of the spike induced by the thalamic input and the intracortical (dendritic) input arising from the local cortical microcircuit of cells with similar stimulus preference. We show that this enhanced response due to dendritic nonlinearity could serve as a mechanism for linear multiplication of thalamocortical signals—amplifying the response to the bottom-up input while maintaining the cells' selectivity (the shape of their tuning curve).

Cortical amplification had been estimated experimentally only in excitatory cells from L4. These cells are not known to generate the BAC firing phenomenon, however, they exhibit dendritic NMDA spikes and are recurrently connected similarly to L5 TTCs (Thomson and Lamy 2007; Lavzin et al. 2012). Recent experimental studies estimated that the recurrent cortical activity amplifies the response rate of L4 cells to thalamic input by a factor of 2–3 without changing the response selectivity (Li, Li et al. 2013; Li, Ibrahim et al. 2013; Lien and Scanziani 2013). Whether this amplification in L4 involves NMDA spikes and/or fine-tuned inhibition (see below) in addition to recurrent excitatory microcircuit activity remains to be determined. Our simulations show that recurrent activity in microcircuits of 150 TTCs resulted in a similar amplification of the response rate (factor of 2.3, unchanged stimulus selectivity), and that the default mode of this amplification relies on dendritic nonlinearities (NMDA and BAC firing). Microcircuits of this size were capable of supplying the dendritic input necessary to trigger BAC firing following a single somatic spike induced by thalamic input. Both NMDA and dendritic Na^+ channels were necessary for the amplification. Thus, the somatic Na^+ spike back-propagated into the dendrites and summated with the dendritic input arriving from other microcircuit cells, triggering NMDA-mediated depolarization and a local dendritic Ca^{2+} spike which, in turn, gave rise to a high-frequency burst of additional Na^+ spikes at the soma, as previously characterized in vitro (Larkum et al. 1999, 2004). Without dendritic excitability, small networks of several hundred cortical cells were capable of only negligible and nonspecific amplification of the single-cell response when isolated, broadening of the response selectivity by nearly 40% (Fig. 6). Thus, our results indicate that dendritic excitability increases the computational power of cortical networks, and in particular is crucial for boosting the activity in microcircuits of similar stimulus preference while maintaining the response selectivity.

The involvement of active dendritic conductance in cortical dynamics is also predicted by recent work on local field potential in a simulated large-scale cortical circuit (Reimann et al. 2013). Future advances in experimental techniques should

enable to selectively block dendritic excitability in the intact brain and thus test our prediction regarding the multiplicative role of dendritic excitability. We note that this mode of cortical modulation could be effectively tuned by targeted dendritic inhibition, for example, inhibition that preferably blocks the dendritic Ca^{2+} spike (Gidon and Segev 2012).

The important role of NMDA currents in modulating cellular response is consistent with previous studies (Schiller et al. 2000; Losonczy and Magee 2006; Lavzin et al. 2012; Smith et al. 2013). Although the feedforward inhibition was sufficient to restrain the microcircuits, it is possible that recurrent inhibition in the simulated microcircuit may restrain the circuit activity sufficiently to necessitate an even larger involvement of NMDA nonlinearities for boosting BAC firing (Larkum et al. 2009). Future studies should explore this possibility by including recurrent inhibition, such as Martinotti interneurons, which form a disynaptic loop with pyramidal cells (Silberberg and Markram 2007). We expect that the main effect of such inclusion would require the activation of larger microcircuits to achieve the same amplification we have observed here. Indeed, large microcircuits under our simplified simulations had an abnormally large spontaneous rate, which would therefore be better restrained by recurrent inhibition. In addition, the tuft-targeting Martinotti cells would allow for a distinct modulation of the contribution of NMDA versus BAC firing to the microcircuit computation.

Detailed understanding of network dynamics in the real biological circuits is largely lacking. For this reason, we have constructed in the present study a simpler network module consisting of local L5 excitatory microcircuit, realistically connected, while simplifying the contribution of the larger network by assuming stochastic background input with reasonable excitatory and inhibitory background synapses, which reproduces the experimentally observed spontaneous firing in TTCs. In our simulations, as in previous studies of recurrent microcircuits (Douglas et al. 1995), background forward inhibition was sufficient to restrain the level of activity in microcircuits that included up to 150 cells. Anatomical and functional studies indicate that the cortical network indeed contains clusters of cells of that size (Perin et al. 2011). Since our microcircuits of 150 cells produced an amplification similar to that observed experimentally in L4, it is possible that the effective local cortical activation involves a similar number of cells. The involvement of finely tailored targeted inhibition, disinhibition, or even neuromodulation (Palmer et al. 2012; Haider et al. 2013; Pfeffer et al. 2013; Polack et al. 2013) should be examined. Future theoretical studies should, therefore, increase the complexity of the network to include feedback inhibition via modeled inhibitory cells (Druckmann et al. 2007). Of particular interest are inhibitory cells that target the distal dendrites in TTCs and thus influencing the coupling between somatic and dendritic spikes (Murayama et al. 2009; Gidon and Segev 2012). In addition, inclusion of $GABA_B$ receptors, which were shown to modulate voltage-gated Ca^{2+} channels (Chalifoux and Carter 2011), will allow for further investigation of means to fine-tune the microcircuit amplification and computation, for example, by switching from full-amplification to partial amplification by NMDA only, similarly to what we have shown by blocking Ca^{2+} channels and NMDA receptors.

The response modulation was robust to temporal jitter (of 10 ms) of the thalamic stimulus. This thalamic jitter is on the order of magnitude observed in most cortical layers during response in vivo (Heimel et al. 2005). Indeed, previous studies show that the highly synchronous thalamic input (Bruno and Sakmann 2006) results in synchronous intracortical inputs (Bruno 2011) and should not involve a large jitter. The robustness of our findings under realistic noisy conditions indicates the robustness of EPSP boosting by BAP as well as BAC firing under such expected jittery conditions in the intact brain, and complements experimental estimates of a time window of 20–30 ms in which the coincident (somatic plus dendritic) stimuli reduce the threshold for the generation of dendritic Ca^{2+} spike (Larkum et al. 1999, 2004).

The coincidence of bottom-up (thalamic) input and dendritic input (originating from both the local circuit as well as from other cortical areas Felleman and Van Essen 1991) in TTCs has been suggested to underlie cognitive associations and perceptual binding of external sensory inputs and internal cortical representations via dendritic nonlinearities (Felleman and Van Essen 1991; Larkum 2012). Our simulations show that the recurrent activity in local cortical microcircuits consisting of 50–150 TTCs provides sufficient coincident dendritic input to trigger dendritic nonlinearities and thus significantly modulate the bottom-up signal. Moreover, replacing the somatic stimulus by a combination of somatic stimulus and dendritic stimulus at the main bifurcation did not change our results (not shown). Future studies should explore how top-down dendritic input, from other cortical areas, may contribute to this modulation, possibly by lowering the threshold for triggering dendritic nonlinearities (Larkum et al. 2009) and thereby increasing the amplification power for a given microcircuit size.

Funding

This study was funded by the Israeli Science Foundation, the EPFL project fund for the Blue Brain Project, an internal fellowship to E. Hay from the Interdisciplinary Center for Neural Computation, and by the Gatsby Charitable Fund. Funding to pay the Open Access publication charges for this article was provided by the above sources.

Notes

Conflict of Interest: None declared.

References

Anderson CT, Sheets PL, Kiritani T, Shepherd GM. 2010. Sublayer-specific microcircuits of corticospinal and corticostriatal neurons in motor cortex. Nat Neurosci. 13:739–744.

Ben-Yishai R, Bar-Or RL, Sompolinsky H. 1995. Theory of orientation tuning in visual cortex. Proc Natl Acad Sci USA. 92:3844–3848.

Binzegger T, Douglas RJ, Martin KA. 2004. A quantitative map of the circuit of cat primary visual cortex. J Neurosci. 24:8441–8453.

Bruno RM. 2011. Synchrony in sensation. Curr Opin Neurobiol. 21:701–708.

Bruno RM, Sakmann B. 2006. Cortex is driven by weak but synchronously active thalamocortical synapses. Science. 312:1622–1627.

Buesing L, Bill J, Nessler B, Maass W. 2011. Neural dynamics as sampling: a model for stochastic computation in recurrent networks of spiking neurons. PLoS Comput Biol. 7:e1002211.

Buonomano DV, Maass W. 2009. State-dependent computations: spatiotemporal processing in cortical networks. Nat Rev Neurosci. 10:113–125.

Carnevale NT, Hines ML. 2006. The NEURON book. Cambridge, UK/New York: Cambridge University Press.

Chalifoux JR, Carter AG. 2011. GABAB receptor modulation of voltage-sensitive calcium channels in spines and dendrites. J Neurosci. 31:4221–4232.
Chance FS, Nelson SB, Abbott LF. 1999. Complex cells as cortically amplified simple cells. Nat Neurosci. 2:277–282.
Constantinople CM, Bruno RM. 2013. Deep cortical layers are activated directly by thalamus. Science. 340:1591–1594.
Constantinople CM, Bruno RM. 2011. Effects and mechanisms of wakefulness on local cortical networks. Neuron. 69:1061–1068.
de Kock CP, Bruno RM, Spors H, Sakmann B. 2007. Layer- and cell-type-specific suprathreshold stimulus representation in rat primary somatosensory cortex. J Physiol. 581:139–154.
Destexhe A, Mainen ZF, Sejnowski TJ. 1994. Synthesis of models for excitable membranes, synaptic transmission and neuromodulation using a common kinetic formalism. J Comput Neurosci. 1:195–230.
Douglas RJ, Koch C, Mahowald M, Martin KA, Suarez HH. 1995. Recurrent excitation in neocortical circuits. Science. 269:981–985.
Douglas RJ, Martin KA. 2007. Mapping the matrix: the ways of neocortex. Neuron. 56:226–238.
Douglas RJ, Martin KA. 2004. Neuronal circuits of the neocortex. Annu Rev Neurosci. 27:419–451.
Druckmann S, Banitt Y, Gidon A, Schurmann F, Markram H, Segev I. 2007. A novel multiple objective optimization framework for constraining conductance-based neuron models by experimental data. Front Neurosci. 1:7–18.
Felleman DJ, Van Essen DC. 1991. Distributed hierarchical processing in the primate cerebral cortex. Cereb Cortex. 1:1–47.
Frick A, Feldmeyer D, Sakmann B. 2007. Postnatal development of synaptic transmission in local networks of L5A pyramidal neurons in rat somatosensory cortex. J Physiol. 585:103–116.
Fuhrmann G, Segev I, Markram H, Tsodyks M. 2002. Coding of temporal information by activity-dependent synapses. J Neurophysiol. 87:140–148.
Gentet LJ, Avermann M, Matyas F, Staiger JF, Petersen CC. 2010. Membrane potential dynamics of GABAergic neurons in the barrel cortex of behaving mice. Neuron. 65:422–435.
Gidon A, Segev I. 2012. Principles governing the operation of synaptic inhibition in dendrites. Neuron. 75:330–341.
Gilbert CD, Wiesel TN. 1979. Morphology and intracortical projections of functionally characterised neurones in the cat visual cortex. Nature. 280:120–125.
Gupta A, Wang Y, Markram H. 2000. Organizing principles for a diversity of GABAergic interneurons and synapses in the neocortex. Science. 287:273–278.
Haider B, Hausser M, Carandini M. 2013. Inhibition dominates sensory responses in the awake cortex. Nature. 493:97–100.
Hay E, Hill S, Schurmann F, Markram H, Segev I. 2011. Models of neocortical layer 5b pyramidal cells capturing a wide range of dendritic and perisomatic active properties. PLoS Comput Biol. 7:e1002107.
Heimel JA, Van Hooser SD, Nelson SB. 2005. Laminar organization of response properties in primary visual cortex of the gray squirrel (*Sciurus carolinensis*). J Neurophysiol. 94:3538–3554.
Heinzle J, Hepp K, Martin KA. 2010. A biologically realistic cortical model of eye movement control in reading. Psychol Rev. 117:808–830.
Heinzle J, Hepp K, Martin KA. 2007. A microcircuit model of the frontal eye fields. J Neurosci. 27:9341–9353.
Helmchen F, Svoboda K, Denk W, Tank DW. 1999. In vivo dendritic calcium dynamics in deep-layer cortical pyramidal neurons. Nat Neurosci. 2:989–996.
Hestrin S. 1992. Activation and desensitization of glutamate-activated channels mediating fast excitatory synaptic currents in the visual cortex. Neuron. 9:991–999.
Hines ML, Morse T, Migliore M, Carnevale NT, Shepherd GM. 2004. ModelDB: a database to support computational neuroscience. J Comput Neurosci. 17:7–11.
Kampa BM, Letzkus JJ, Stuart GJ. 2006. Cortical feed-forward networks for binding different streams of sensory information. Nat Neurosci. 9:1472–1473.
Ko H, Hofer SB, Pichler B, Buchanan KA, Sjostrom PJ, Mrsic-Flogel TD. 2011. Functional specificity of local synaptic connections in neocortical networks. Nature. 473:87–91.
Larkum M. 2012. A cellular mechanism for cortical associations: an organizing principle for the cerebral cortex. Trends Neurosci. 36:141–151.
Larkum ME, Nevian T, Sandler M, Polsky A, Schiller J. 2009. Synaptic integration in tuft dendrites of layer 5 pyramidal neurons: a new unifying principle. Science. 325:756–760.
Larkum ME, Senn W, Luscher HR. 2004. Top-down dendritic input increases the gain of layer 5 pyramidal neurons. Cereb Cortex. 14:1059–1070.
Larkum ME, Zhu JJ. 2002. Signaling of layer 1 and whisker-evoked Ca^{2+} and Na^{+} action potentials in distal and terminal dendrites of rat neocortical pyramidal neurons in vitro and in vivo. J Neurosci. 22:6991–7005.
Larkum ME, Zhu JJ, Sakmann B. 1999. A new cellular mechanism for coupling inputs arriving at different cortical layers. Nature. 398:338–341.
Lavzin M, Rapoport S, Polsky A, Garion L, Schiller J. 2012. Nonlinear dendritic processing determines angular tuning of barrel cortex neurons in vivo. Nature. 490:397–401.
Li YT, Ibrahim LA, Liu BH, Zhang LI, Tao HW. 2013. Linear transformation of thalamocortical input by intracortical excitation. Nat Neurosci. 16:1324–1330.
Li LY, Li YT, Zhou M, Tao HW, Zhang LI. 2013. Intracortical multiplication of thalamocortical signals in mouse auditory cortex. Nat Neurosci. 16:1179–1181.
Lien AD, Scanziani M. 2013. Tuned thalamic excitation is amplified by visual cortical circuits. Nat Neurosci. 16:1315–1323.
Litvak S, Ullman S. 2009. Cortical circuitry implementing graphical models. Neural Comput. 21:3010–3056.
Liu BH, Wu GK, Arbuckle R, Tao HW, Zhang LI. 2007. Defining cortical frequency tuning with recurrent excitatory circuitry. Nat Neurosci. 10:1594–1600.
Losonczy A, Magee JC. 2006. Integrative properties of radial oblique dendrites in hippocampal CA1 pyramidal neurons. Neuron. 50:291–307.
Markram H, Lubke J, Frotscher M, Roth A, Sakmann B. 1997. Physiology and anatomy of synaptic connections between thick tufted pyramidal neurones in the developing rat neocortex. J Physiol. 500(Pt 2):409–440.
Meyer HS, Wimmer VC, Hemberger M, Bruno RM, de Kock CP, Frick A, Sakmann B, Helmstaedter M. 2010. Cell type-specific thalamic innervation in a column of rat vibrissal cortex. Cereb Cortex. 20:2287–2303.
Murayama M, Perez-Garci E, Nevian T, Bock T, Senn W, Larkum ME. 2009. Dendritic encoding of sensory stimuli controlled by deep cortical interneurons. Nature. 457:1137–1141.
Olsen SR, Bortone DS, Adesnik H, Scanziani M. 2012. Gain control by layer six in cortical circuits of vision. Nature. 483:47–52.
Palmer LM, Schulz JM, Murphy SC, Ledergerber D, Murayama M, Larkum ME. 2012. The cellular basis of GABA(B)-mediated interhemispheric inhibition. Science. 335:989–993.
Palmer LM, Shai AS, Reeve JE, Anderson HL, Paulsen O, Larkum ME. 2014. NMDA spikes enhance action potential generation during sensory input. Nat Neurosci. 17:383–390.
Papoutsi A, Sidiropoulou K, Cutsuridis V, Poirazi P. 2013. Induction and modulation of persistent activity in a layer V PFC microcircuit model. Front Neural Circuits. 7:161.
Perin R, Berger TK, Markram H. 2011. A synaptic organizing principle for cortical neuronal groups. Proc Natl Acad Sci USA. 108:5419–5424.
Pfeffer CK, Xue M, He M, Huang ZJ, Scanziani M. 2013. Inhibition of inhibition in visual cortex: the logic of connections between molecularly distinct interneurons. Nat Neurosci. 16:1068–1076.
Polack PO, Friedman J, Golshani P. 2013. Cellular mechanisms of brain state-dependent gain modulation in visual cortex. Nat Neurosci. 16:1331–1339.
Polsky A, Mel BW, Schiller J. 2004. Computational subunits in thin dendrites of pyramidal cells. Nat Neurosci. 7:621–627.
Polsky A, Mel B, Schiller J. 2009. Encoding and decoding bursts by NMDA spikes in basal dendrites of layer 5 pyramidal neurons. J Neurosci. 29:11891–11903.

Ramaswamy S, Hill SL, King JG, Schurmann F, Wang Y, Markram H. 2012. Intrinsic morphological diversity of thick-tufted layer 5 pyramidal neurons ensures robust and invariant properties of in silico synaptic connections. J Physiol. 590:737–752.
Reimann MW, Anastassiou CA, Perin R, Hill SL, Markram H, Koch C. 2013. A biophysically detailed model of neocortical local field potentials predicts the critical role of active membrane currents. Neuron. 79:375–390.
Reyes A, Sakmann B. 1999. Developmental switch in the short-term modification of unitary EPSPs evoked in layer 2/3 and layer 5 pyramidal neurons of rat neocortex. J Neurosci. 19:3827–3835.
Rhodes P. 2006. The properties and implications of NMDA spikes in neocortical pyramidal cells. J Neurosci. 26:6704–6715.
Ringach DL, Shapley RM, Hawken MJ. 2002. Orientation selectivity in macaque V1: diversity and laminar dependence. J Neurosci. 22:5639–5651.
Salin PA, Prince DA. 1996. Electrophysiological mapping of GABAA receptor-mediated inhibition in adult rat somatosensory cortex. J Neurophysiol. 75:1589–1600.
Sarid L, Bruno R, Sakmann B, Segev I, Feldmeyer D. 2007. Modeling a layer 4-to-layer 2/3 module of a single column in rat neocortex: interweaving in vitro and in vivo experimental observations. Proc Natl Acad Sci USA. 104:16353–16358.
Schiller J, Major G, Koester HJ, Schiller Y. 2000. NMDA spikes in basal dendrites of cortical pyramidal neurons. Nature. 404:285–289.
Schiller J, Schiller Y. 2001. NMDA receptor-mediated dendritic spikes and coincident signal amplification. Curr Opin Neurobiol. 11: 343–348.
Silberberg G, Markram H. 2007. Disynaptic inhibition between neocortical pyramidal cells mediated by Martinotti cells. Neuron. 53: 735–746.
Smith SL, Smith IT, Branco T, Hausser M. 2013. Dendritic spikes enhance stimulus selectivity in cortical neurons in vivo. Nature. 503:115–120.
Song S, Sjostrom PJ, Reigl M, Nelson S, Chklovskii DB. 2005. Highly nonrandom features of synaptic connectivity in local cortical circuits. PLoS Biol. 3:e68.
Stuart GJ, Hausser M. 2001. Dendritic coincidence detection of EPSPs and action potentials. Nat Neurosci. 4:63–71.
Suarez H, Koch C, Douglas R. 1995. Modeling direction selectivity of simple cells in striate visual cortex within the framework of the canonical microcircuit. J Neurosci. 15:6700–6719.
Takahashi H, Magee JC. 2009. Pathway interactions and synaptic plasticity in the dendritic tuft regions of CA1 pyramidal neurons. Neuron. 62:102–111.
Thomson AM, Lamy C. 2007. Functional maps of neocortical local circuitry. Front Neurosci. 1:19–42.
Traub RD, Contreras D, Cunningham MO, Murray H, LeBeau FE, Roopun A, Bibbig A, Wilent WB, Higley MJ, Whittington MA. 2005. Single-column thalamocortical network model exhibiting gamma oscillations, sleep spindles, and epileptogenic bursts. J Neurophysiol. 93:2194–2232.
Tsodyks MV, Markram H. 1997. The neural code between neocortical pyramidal neurons depends on neurotransmitter release probability. Proc Natl Acad Sci USA. 94:719–723.
Vaidya SP, Johnston D. 2013. Temporal synchrony and gamma-to-theta power conversion in the dendrites of CA1 pyramidal neurons. Nat Neurosci. 16:1812–1820.
Van Hooser SD. 2007. Similarity and diversity in visual cortex: is there a unifying theory of cortical computation? Neuroscientist. 13: 639–656.
Williams SR, Atkinson SE. 2007. Pathway-specific use-dependent dynamics of excitatory synaptic transmission in rat intracortical circuits. J Physiol. 585:759–777.
Xu NL, Harnett MT, Williams SR, Huber D, O'Connor DH, Svoboda K, Magee JC. 2012. Nonlinear dendritic integration of sensory and motor input during an active sensing task. Nature. 492:247–251.
Yoshimura Y, Callaway EM. 2005. Fine-scale specificity of cortical networks depends on inhibitory cell type and connectivity. Nat Neurosci. 8:1552–1559.
Yoshimura Y, Dantzker JL, Callaway EM. 2005. Excitatory cortical neurons form fine-scale functional networks. Nature. 433:868–873.